

## Supplementary Information

### **Modification of 2D Materials using MoS<sub>2</sub> as a Model for Investigating Al-Storage Properties on Diverse Crystal Facets**

Rongkai Kang, Yiqun Du, Dongmei Zhang, Chenyi Sun, Wei Zhou, Han Wang,

Guowen Chen\*, Jianxin Zhang\*

Key Laboratory for Liquid-Solid Structural Evolution and Processing of Materials  
(Ministry of Education), School of Materials Science and Engineering, Shandong  
University, Jinan 250061, China

#### **\*Corresponding Authors**

E-mail addresses (Guowen Chen): [cgw@sdu.edu.cn](mailto:cgw@sdu.edu.cn)

E-mail addresses (Jianxin Zhang): [jianxin@sdu.edu.cn](mailto:jianxin@sdu.edu.cn)

## **Experimental Section**

### **Preparations of S-MoS<sub>2</sub> and MoS<sub>2</sub>**

The C<sub>3</sub>H<sub>6</sub>N<sub>6</sub> was heated at 550 °C for 4 h to obtain C<sub>3</sub>N<sub>4</sub>. Then, the C<sub>3</sub>N<sub>4</sub>, (NH<sub>4</sub>)<sub>2</sub>MoO<sub>4</sub>, and CH<sub>4</sub>N<sub>2</sub>S were ball milled for 2 h in a weight ratio of 10:1:2. The sample was heated at 550 °C for 4 h in Ar atmosphere to generate MoS<sub>2</sub>, and further heated to 800 °C for 2 h to volatilize C<sub>3</sub>N<sub>4</sub>. After cooling, the S-MoS<sub>2</sub> was obtained. As a control, MoS<sub>2</sub> was synthesized by the same method as S-MoS<sub>2</sub> except for the presence of C<sub>3</sub>N<sub>4</sub>.

### **Material characterizations**

The phase structure of samples was investigated in the sweep range of 10-80 degrees by X-ray diffraction (XRD, Rigaku Smartlab SE). The morphology and microstructure information were performed by field-emission scanning electron microscopy (SEM, JEOL JSM-7800F) and transmission electron microscopy (TEM, JEOL JEM-2100). The surface valance states were characterized using X-ray photoelectron spectroscopy (Krayos AXIS Ultra DLD). N<sub>2</sub> adsorption-desorption tests were implemented to determine the surface area and pore size of samples by ASAP 2420.

### **Electrochemical performance tests**

The active materials (80%), acetylene black (10%), and PVDF (10%) were mixed with N-methyl pyrrolidone as a solvent and kept stirring for 12 h. The resulting slurry was coated on the current collector (Mo foil) and vacuum dried at 60 °C for 12 h. The mass loading of cathode was 1.0-1.2 mg cm<sup>-2</sup>. High-purity Al foil and glass-fiber

membrane were used as reference electrode and separator, respectively. A fixed amount of ionic liquid (80  $\mu\text{L}$ ) composed of  $\text{AlCl}_3$  and  $[\text{EMIm}]\text{Cl}$  with a molar ratio of 1.1:1 was used as the electrolyte of batteries. The electrochemical performance of cathode materials was tested using the assembled 2025-type coin cells. The smaller amount of electrolyte and the lower concentration of  $\text{AlCl}_3$  avoid the side reaction between the electrolyte and stainless steel coin cells. Cyclic voltammogram (CV) curves for current collector without active material are shown in Figure S13, showing that no significant redox reaction is experienced between the coin cells and the electrolyte. The CV test was performed on an electrochemical workstation (CHI 660E) with a scanning rate of  $0.5 \text{ mV s}^{-1}$ . In GITT tests, each discharge pulse lasted for 3 min at current density of  $100 \text{ mA g}^{-1}$  and relaxation time was 1 min. Electrochemical impedance spectroscopy (EIS) was performed on the same electrochemical workstation with a frequency range of 100,000 to 0.01 Hz. Galvanostatic charge/discharge performance was tested by the Land CT2001A system in a voltage range of 0.01-1.8 V.

### **First-principles calculations**

The first-principles calculations were implemented by Vienna Ab initio Simulation Package (VASP) based on density functional theory (DFT). The exchange-correlation function of electrons was explained using generalized gradient approximation (GGA) with the Perdew-Burke-Ernzerhof (PBE) function. The core-valence interaction was performed on the projector augmented-wave (PAW) method. The (001), interlayer, and (100) planes of  $\text{MoS}_2$  were cleaved to interact with the  $\text{Al}^{3+}$  and  $\text{AlCl}_4^-$  ions. The vacuum region was 16 Å. The cutoff energy was 300 eV and the

k-point mesh was used  $3 \times 3 \times 1$ . The convergence of energy was set to  $1 \times 10^{-5}$  eV.

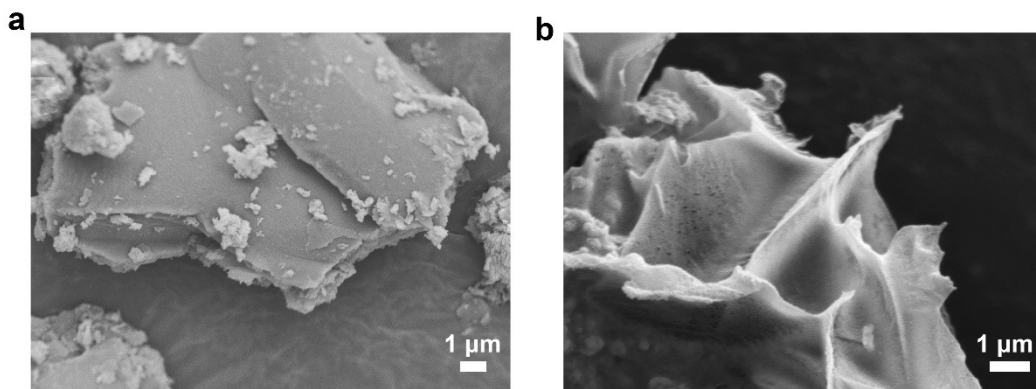


**Figure S1.** SEM images of (a)  $C_3N_4$  and (b)  $MoS_2$ .

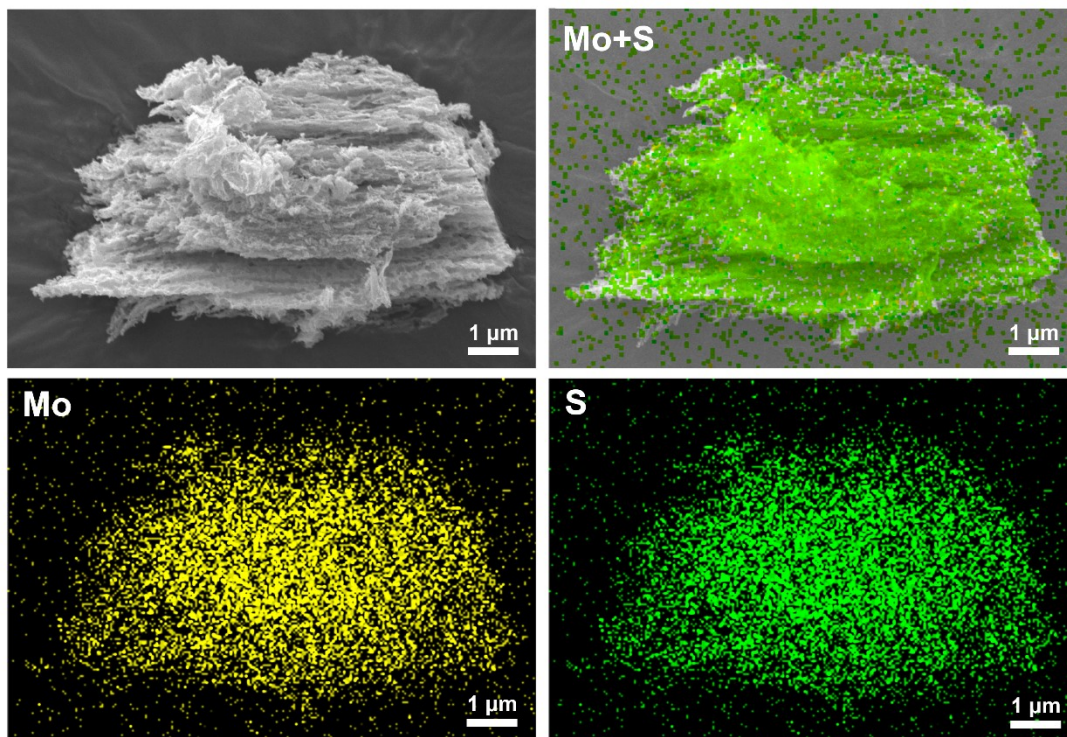


**Figure S2.** Elemental mapping images of S-MoS<sub>2</sub>.

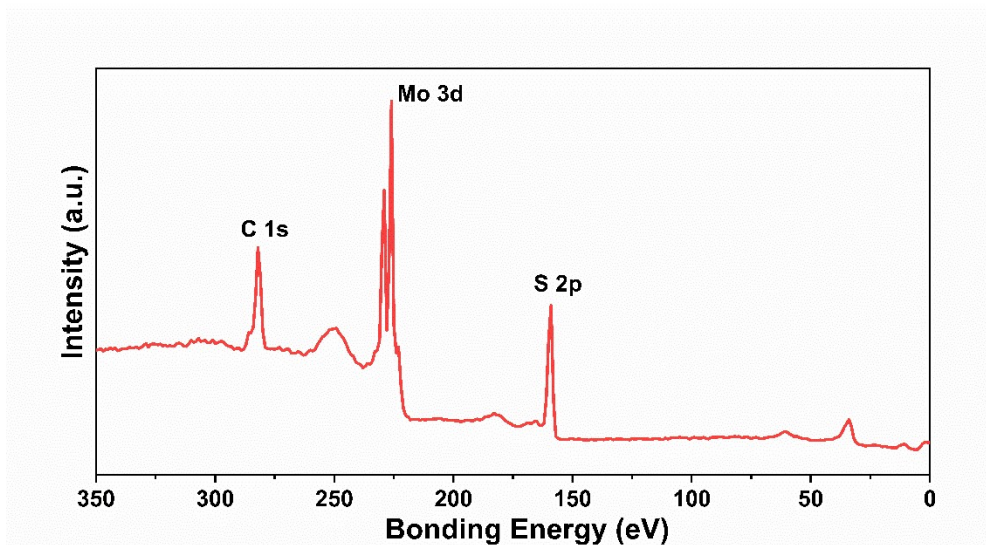


**Figure S3.** XPS full scan survey of S-MoS<sub>2</sub>.

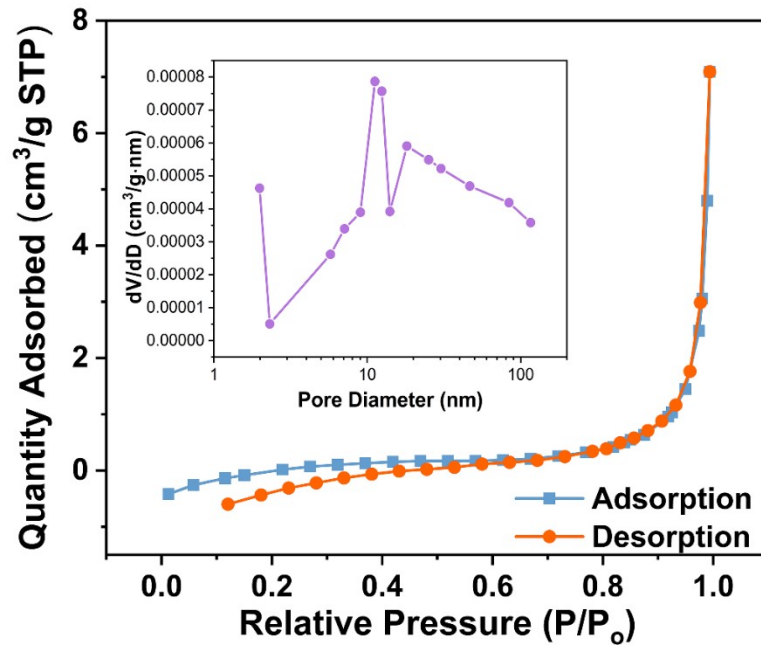
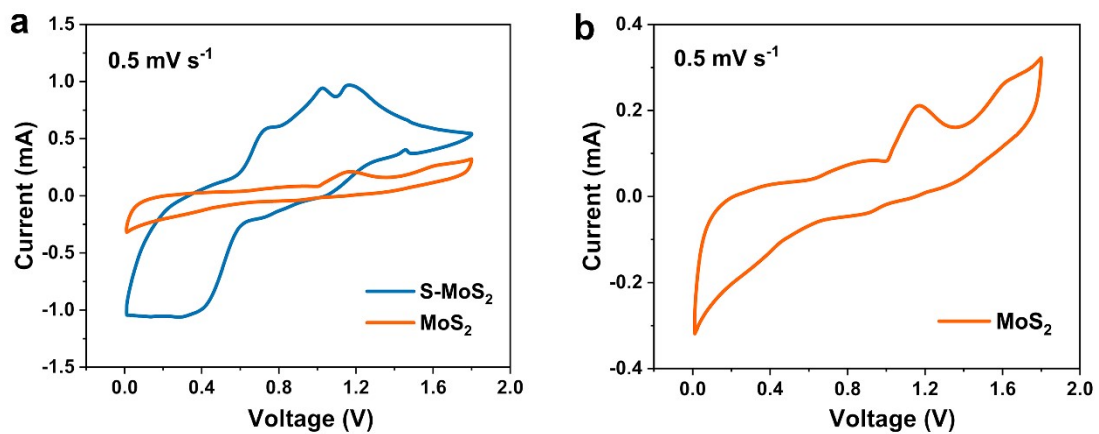
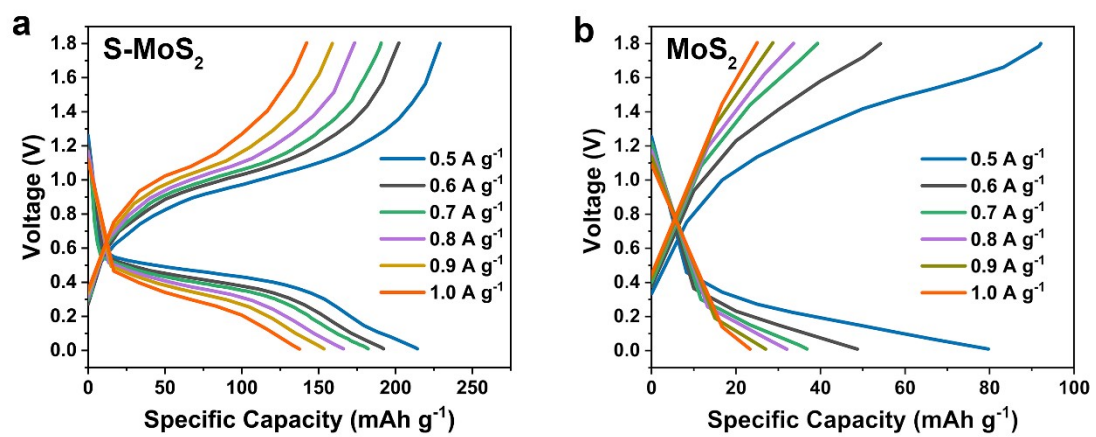


Figure S4. N<sub>2</sub> adsorption-desorption curves of MoS<sub>2</sub>.



**Figure S5.** CV curves of (a) S-MoS<sub>2</sub> and MoS<sub>2</sub> and (b) MoS<sub>2</sub> at a scan rate of  $0.5 \text{ mV s}^{-1}$ .



**Figure S6.** Charge-discharge curves of (a) S-MoS<sub>2</sub> and (b) MoS<sub>2</sub> at various current densities.

Strategy	Capacity (mAh g <sup>-1</sup> )	Cycle (number)	Current density (A g <sup>-1</sup> )	Reference
S-MoS <sub>2</sub>	167	100	1	This work
	129	1000	2	
C4Q	102	500	0.2	[1]
Co <sub>3</sub> Se <sub>4</sub> /ZnSe	117	500	0.2	[2]
VS <sub>4</sub> -PH10	300	100	0.2	[3]
Al <sub>2/3</sub> Li <sub>1/3</sub> Mn <sub>2</sub> O <sub>4</sub>	93	1000	1	[4]
S-WSe <sub>2</sub>	110	1500	2	[5]
Natural graphite	60	6000	0.66	[6]
CoSe	63	100	5	[7]
Co <sub>3</sub> O <sub>4</sub>	116	500	0.5	[8]
V <sub>2</sub> O <sub>5</sub> /C	75	30	0.02	[9]
CoFe <sub>2</sub> O <sub>4</sub> @rGO	67	500	1	[10]
δ-MnO <sub>2</sub>	37	100	0.1	[11]
G-SnS <sub>2</sub>	70	100	0.2	[12]
CuS@C	90	100	0.02	[13]
WS <sub>2</sub>	119	500	1	[14]
VS <sub>4</sub> /rGO	60	100	0.3	[15]
SnSe	107	100	0.3	[16]
graphite flakes	100	300	0.6	[17]
graphite nanoflakes	57	300	0.1	[18]
S-NiCo@rGO	83	100	1	[19]
cobalt sulfide nanosheets	120	250	0.2	[20]
crystal carbon@graphene	100	300	1	[21]
Porous CuO	112	100	0.2	[22]
V <sub>2</sub> CT <sub>x</sub> MXene	80	100	0.2	[23]
Ni <sub>3</sub> S <sub>2</sub> @Graphene	50	300	0.2	[24]
Co <sub>3</sub> S <sub>4</sub>	90	150	0.05	[25]
Zn/Co-Se@C	79	400	1	[26]
NiCoSe <sub>2</sub> @F-C	115	400	1	[27]□

**Table S1.** Comparison of S-MoS<sub>2</sub> and other reported cathode materials in ABs.

Strategy	Capacity (mAh g <sup>-1</sup> )	Cycle (number)	Current density (A g <sup>-1</sup> )	Reference
S-MoS <sub>2</sub>	167	100	1	This work
	129	1000	2	
MoS <sub>2</sub> /Polythiophene	80	40	0.075	[28]
Few-layered ultra-small MoS <sub>2</sub>	80	150	0.1	[29]
MoS <sub>2</sub> -RGO	150	100	1	[30]
MoS <sub>2</sub>	43	/	0.04	[31]

**Table S2.** Comparison of S-MoS<sub>2</sub> and MoS<sub>2</sub>-based cathode reported in ABs.

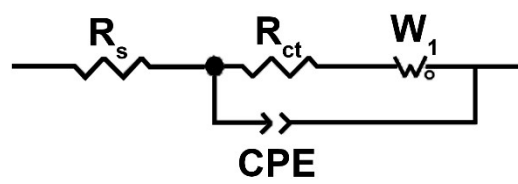


**Figure S7.** The equivalent circuit diagram of EIS tests.

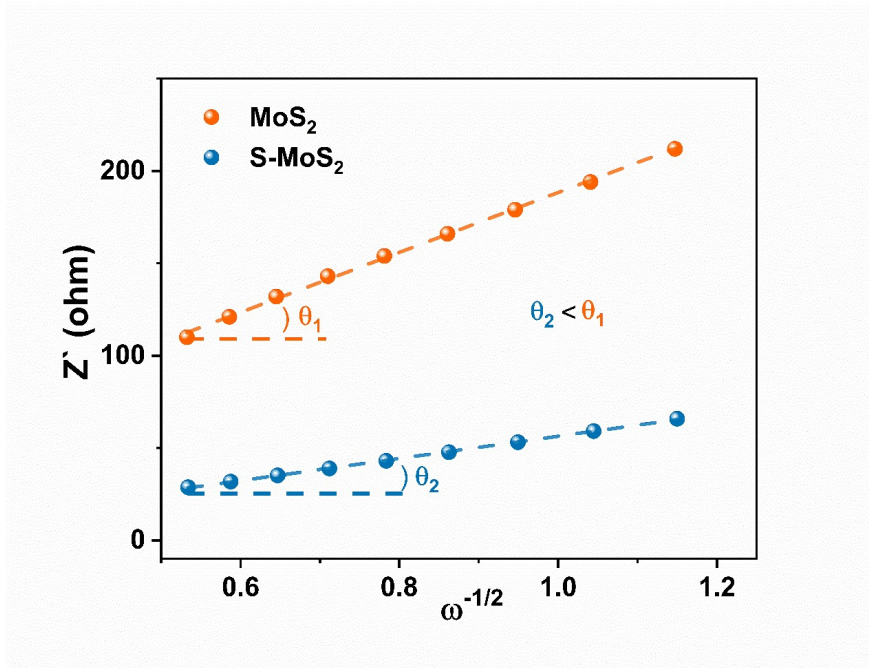
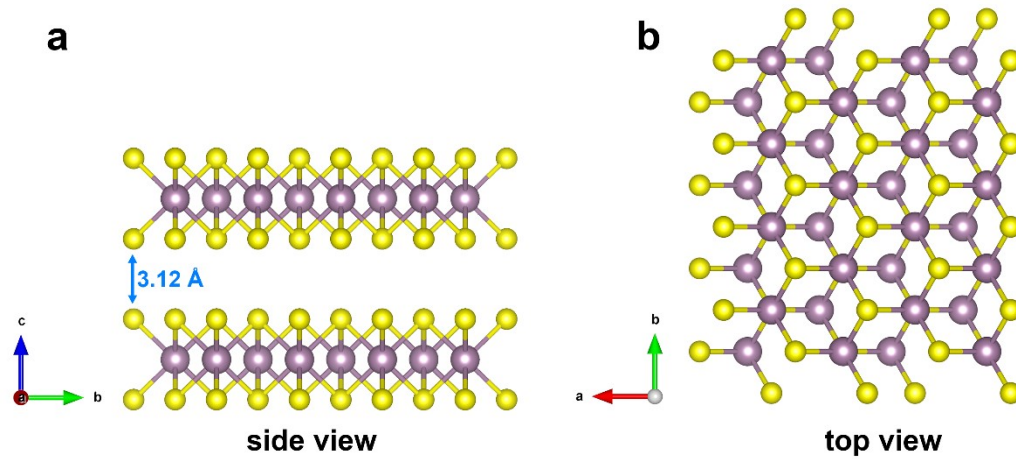


Figure S8. Relationships between  $Z'$  and  $\omega^{-1/2}$  for S-MoS<sub>2</sub> and MoS<sub>2</sub> cathodes.

State	1T (%)	2H (%)
Pristine	55.3	28.5
1 <sup>st</sup> discharge	21.6	63.7
1 <sup>st</sup> charge	47.7	36.9

**Table S3.** The proportion of 1T phase and 2H phase in S-MoS<sub>2</sub> at different voltage states.



**Figure S9.** (a) Side view and (b) top view of the pristine MoS<sub>2</sub> crystal model.

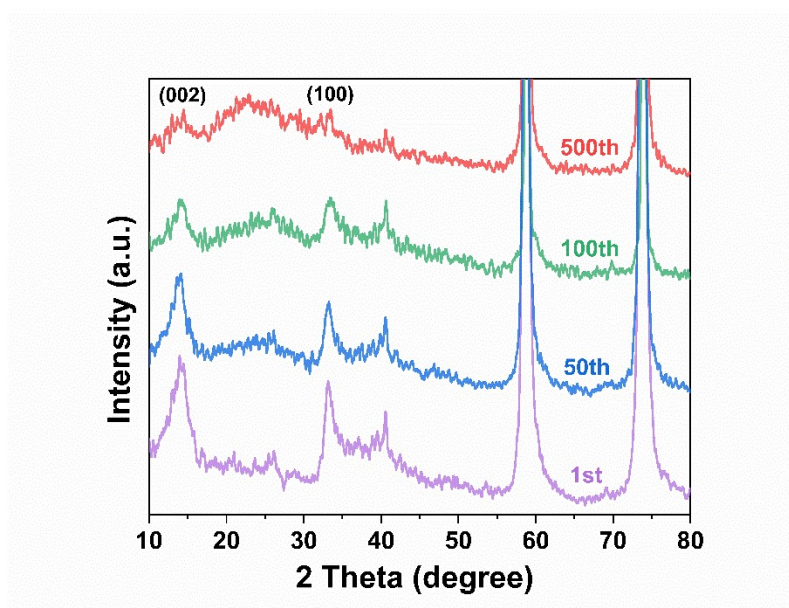


**Figure S10.** Ex-situ XRD patterns of MoS<sub>2</sub> cathode after cycling at 2A g<sup>-1</sup>.

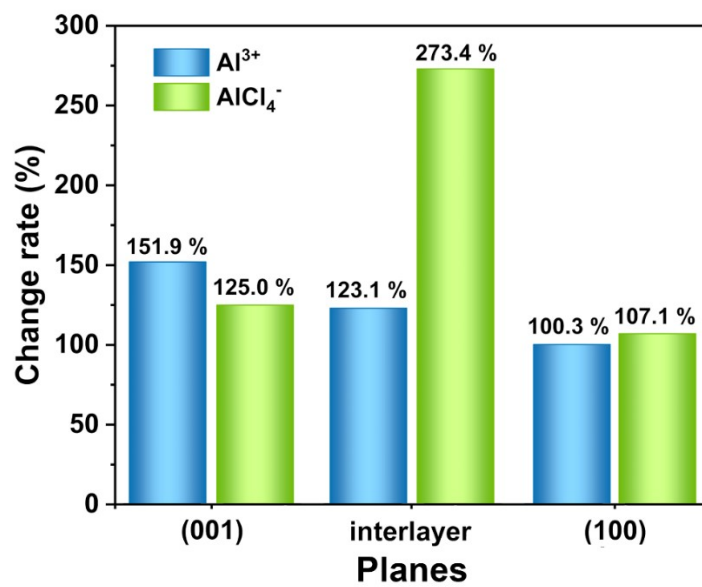


**Figure S11.** Comparison of lattice change rates for  $\text{Al}^{3+}$  and  $\text{AlCl}_4^-$  on different facets.

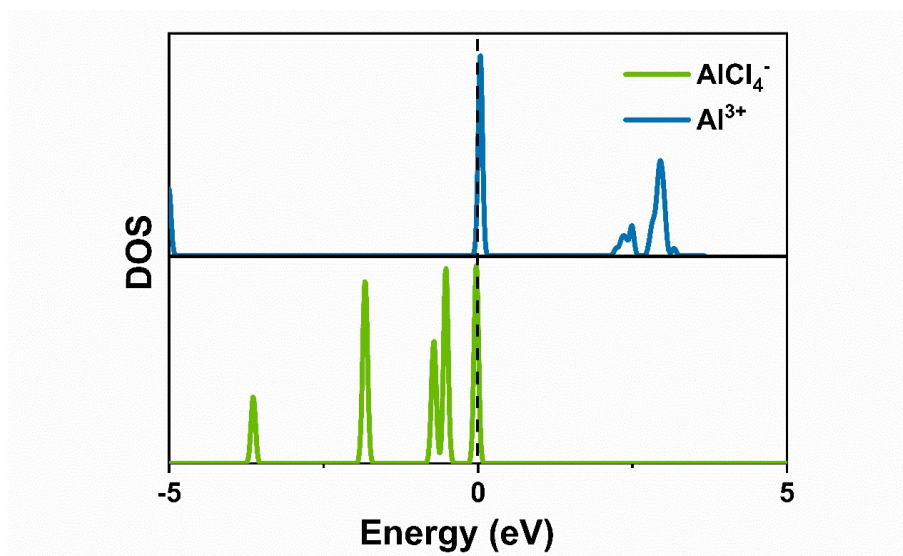
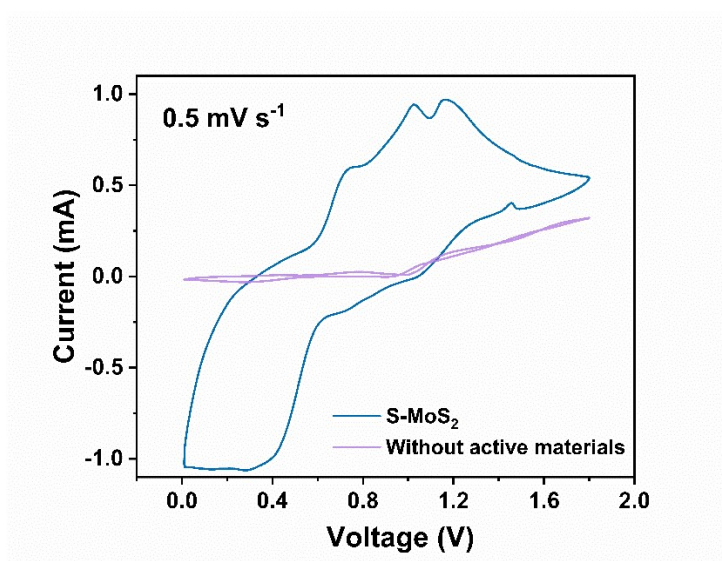


Figure S12. DOS of  $\text{Al}^{3+}$  and  $\text{AlCl}_4^-$ .



**Figure S13.** CV curve of cathode without active material shows no significant redox reaction between coin cell and electrolyte.

## References:

- 1 M. Han, Q. Zhou, M. Zhang, J. Wang, F. Cui, Y. Yang, J. Su, W. Huang, Y. Hu, *J. Mater. Chem. A Mater.*, 2023.
- 2 T. Liu, G. Lv, M. Liu, C. Zhao, L. Liao, H. Liu, J. Shi, J. Zhang, J. Guo, *ACS Appl. Mater. Interfaces*, 2023, **15**, 11906-11913.
- 3 X. Han, F. Wu, R. Zhao, Y. Bai, C. Wu, *ACS Appl. Mater. Interfaces*, 2023, **15**, 6888-6901.
- 4 R. Li, C. Xu, X. Wu, J. Zhang, X. Yuan, F. Wang, Q. Yao, M. Sadeeq (Jie Tang) Balogun, Z. Lu, J. Deng, *Energy Storage Mater.*, 2022, **53**, 514-522.
- 5 F. Cui, M. Han, W. Zhou, C. Lai, Y. Chen, J. Su, J. Wang, H. Li, Y. Hu, *Small Methods*, 2022, **6**, 2201281.
- 6 D. Y. Wang, C. Y. Wei, M. C. Lin, C. J. Pan, H. L. Chou, H. A. Chen, M. Gong, Y. Wu, C. Yuan, M. Angell, Y. J. Hsieh, Y. H. Chen, C. Y. Wen, C. W. Chen, B. J. Hwang, C. C. Chen, H. Dai, *Nat. Commun.*, 2017, **8**, 14283.
- 7 W. Xing, D. Du, T. Cai, X. Li, J. Zhou, Y. Chai, Q. Xue, Z. Yan, *J. Power Sources*, 2018, **401**, 6-12.
- 8 Z. Li, W. Lv, G. Wu, X. Li, X. Wang, W. Zhang, *Chem. Eng. J.*, 2022, **430**, 133135.
- 9 M. Chiku, H. Takeda, S. Matsumura, E. Higuchi, H. Inoue, *ACS Appl. Mater. Interfaces*, 2015, **7**, 24385-24389.
- 10 K. Zhang, T. H. Lee, J. H. Cha, H. W. Jang, J.-W. Choi, M. Mahmoudi, M. Shokouhimehr, *Sci. Rep.*, 2019, **9**, 13739.
- 11 P. Almodóvar, D. A. Giraldo, J. Chancón, I. Álvarez-Serrano, M. L. López, *ChemElectroChem*, 2020, **7**, 2102-2106.
- 12 Y. Hu, B. Luo, D. Ye, X. Zhu, M. Lyu, L. Wang, *Adv. Mater.*, 2017, **29**, 1606132.
- 13 S. Wang, S. Jiao, J. Wang, H.-S. Chen, D. Tian, H. Lei, D.-N. Fang, *ACS Nano*, 2017, **11**, 469-477.
- 14 Z. Zhao, Z. Hu, Q. Li, H. Li, X. Zhang, Y. Zhuang, F. Wang, G. Yu, *Nano Today*, 2020, **32**, 100870.
- 15 X. Zhang, S. Wang, J. Tu, G. Zhang, S. Li, D. Tian, S. Jiao, *ChemSusChem*, 2018, **11**, 709-715.
- 16 Y. Zhang, B. Zhang, J. Li, J. Liu, X. Huo, F. Kang, *Chem. Eng. J.*, 2021, **403**, 126377.
- 17 C. Liu, Z. Liu, Q. Li, H. Niu, C. Wang, Z. Wang, B. Gao, *J Power Sources*, 2019, **438**, 226950.
- 18 J. Tu, J. Wang, S. Li, W.-L. Song, M. Wang, H. Zhu, S. Jiao, *Nanoscale*, 2019, **11**, 12537-12546.
- 19 W. Xing, X. Li, T. Cai, Y. Zhang, P. Bai, J. Xu, H. Hu, M. Wu, Q. Xue, Y. Zhao,

- J. Zhou, S. Zhuo, X. Gao, Z. Yan, *Electrochim. Acta*, 2020, **344**, 136174.
- 20 Z. Hu, K. Zhi, Q. Li, Z. Zhao, H. Liang, X. Liu, J. Huang, C. Zhang, H. Li, X. Guo, *J. Power Sources*, 2019, **440**, 227147.
- 21 Z. Liu, J. Wang, X. Jia, W. Li, Q. Zhang, L. Fan, H. Ding, H. Yang, X. Yu, X. Li, B. Lu, *ACS Nano*, 2019, **13**, 10631-10642.
- 22 X. Zhang, G. Zhang, S. Wang, S. Li, S. Jiao, *J. Mater. Chem. A. Mater.*, 2018, **6**, 3084-3090.
- 23 A. VahidMohammadi, A. Hadjikhani, S. Shahbazmohamadi, M. Beidaghi, *ACS Nano*, 2017, **11**, 11135-11144.
- 24 S. Wang, Z. Yu, J. Tu, J. Wang, D. Tian, Y. Liu, S. Jiao, *Adv. Energy Mater.*, 2016, **6**, 1600137.
- 25 H. Li, H. Yang, Z. Sun, Y. Shi, H. M. Cheng, F. Li, *Nano Energy*, 2019, **56**, 100-108.
- 26 Z. Li, W. Lv, G. Wu, W. Zhang, *J. Power Sources*, 2021, **511**, 230455.
- 27 R. Kang, Y. Du, W. Zhou, D. Zhang, W. Zhang, J. Wan, G. Chen, J. Zhang, *ACS Appl. Energy Mater.*, 2022, **5**, 10287-10296.
- 28 V. Raju, V. N. Kumar Y, V. R. Jetti, P. Basak, *ACS Appl. Energy Mater.*, 2021, **4**, 9227-9239.
- 29 Q. Zhang, Q. Liu, E. Wang, *Sustain Energy Fuels*, 2021, **5**, 4289-4294.
- 30 B. Tan, S. Han, W. Luo, Z. Chao, J. Fan, M. Wang, *J. Alloys Compd.*, 2020, **841**, 155732.
- 31 S. Divya, J. H. Johnston, T. Nann, *Energy Technology*, 2020, **8**, 2000038.